Contrib Mineral Petrol (2011) 162:1079–1092
DOI 10.1007/s00410-011-0641-4

ORIGINAL PAPER

Oxygen isotope variations of garnets and clinopyroxenes in a layered diamondiferous calcsilicate rock from Kokchetav Massif, Kazakhstan: a window into the geochemical nature of deeply subducted UHPM rocks

N. V. Sobolev · H.-P. Schertl · J. W. Valley · F. Z. Page · N. T. Kita · M. J. Spicuzza · R. D. Neuser · A. M. Logvinova

Received: 6 November 2009 / Accepted: 21 April 2011 / Published online: 13 May 2011

Abstract Calcsilicate and garnet-pyroxene rocks with dolomite and Mg-calcite matrices occur with UHPM diamondiferous biotite gneisses and schists of the Kokchetav Massif. The calcsilicates are characterized by high diamond grade, K-bearing diopside, and very high Mg-garnets (Mg# > 77) with variable Ca contents (Ca# = 42.5–80). A rare calcsilicate sample with alternating layers of different bulk compositions was selected for oxygen isotope and electron probe microanalysis of garnets and pyroxenes. A grain of fresh garnet with a brownish-yellow luminescent inner domain (Mg# 94) and a non-luminescent outer part (Mg# 88) was selected for in situ analysis of $\delta^{18}O$ by ion microprobe (10 μm spot). The profile demonstrates a $\delta^{18}O$ gradient of 1.5‰/200 μm, from 11.3 (rim) to 12.8‰ (core) VSMOW. Additional 2 mg samples of hand-picked garnet and clinopyroxene fragments from different parts of the same sample (selected by color and chemical differences) were analyzed for $\delta^{18}O$ by laser fluorination, yielding even larger differences in $\delta^{18}O$: 6.3–10.6‰ in garnets and 6.1–8.1 in clinopyroxenes. The zonation in $\delta^{18}O$ among grains of the same mineral in different lithologies may in part reflect initial heterogeneities of the finely layered sedimentary precursors. The $\delta^{18}O$ values for the garnets are among the highest observed for UHP-origin (both for crustal or mantle rocks), confirming a sedimentary origin for these carbonate-bearing rocks, and ruling out a primitive mantle-derived protolith. Oxygen diffusion in garnet at peak metamorphism temperature (1,000°C) was arrested by rapid cooling.

Keywords Kokchetav Massif · Garnet · Pyroxene · Oxygen isotopes · Ultrahigh pressure · Ion microprobe

Communicated by J. Hoefs.

Electronic supplementary material The online version of this article (doi:10.1007/s00410-011-0641-4) contains supplementary material, which is available to authorized users.

N. V. Sobolev · A. M. Logvinova
V.S. Sobolev Institute of Geology and Mineralogy, Siberian Branch of Russian Academy of Sciences, 630090 Novosibirsk 90, Russia

H.-P. Schertl (✉) · R. D. Neuser
Institut für Geologie, Mineralogie, und Geophysik, Ruhr-Universität Bochum, 44780 Bochum, Germany
e-mail: hans-peter.schertl@rub.de

J. W. Valley · F. Z. Page · N. T. Kita · M. J. Spicuzza
WiscSIMS Laboratory, Department of Geoscience, University of Wisconsin, Madison, WI 53706, USA

Present Address:
F. Z. Page
Department of Geology, Oberlin College, Oberlin, OH 44074, USA

Introduction

The presence of coesite and diamond, associated with Mg-rich garnets and K-bearing clinopyroxenes, makes some crust-derived ultrahigh pressure metamorphic (UHPM) rocks resemble those of mantle origin. Likewise, inclusions of garnet and pyroxene in kimberlitic diamonds of magmatic origin can be very similar to those associated with UHPM diamonds (e.g., Chopin and Sobolev 1995). Indeed, the first evidence of coesite eclogites in the upper mantle came from the discovery of coesite, garnet, and clinopyroxene inclusions in Siberian diamonds from placer deposits, which are interpreted to be derived from kimberlitic sources (Sobolev et al. 1976). Low carbon isotope ratios in these and other diamonds (Sobolev et al. 1979)

were explained by their close relationship to the subducted oceanic crust (Sobolev and Sobolev 1980). In order to distinguish between crustal or mantle origin of garnet-pyroxene rocks and some peridotites, a study of the mineralogical and geochemical features is required. It is important to note that garnets in high temperature equilibrium with primitive mantle material have a narrow range in $\delta^{18}O$ (5.3 ± 0.6‰, 2SD, Valley et al. 1998; Valley 2003). Likewise, Mattey et al. (1994) reported values of 5.2‰ for olivines and garnets from selected peridotites and estimated $\delta^{18}O = 5.5 \pm 0.8$‰ (2SD) for the whole-rock value of average mantle peridotites. Similar values are reported by Schulze et al. (2001) for garnet megacrysts from kimberlites worldwide (average $\delta^{18}O = 5.24$‰, $n = 121$). The fractionation of oxygen isotope ratios is very small at magmatic temperatures and values of $\delta^{18}O$ significantly *outside* this narrow 1.2‰ "mantle range" (5.3 ± 0.6) only form at lower temperatures in the crust where fractionations are large. The converse does not hold, however, and values *within* the mantle range are common in both the crust and mantle. Thus, oxygen isotope ratios of garnet and other minerals, if they are outside the mantle range, are signatures for a crustal input and can help resolve controversy on the origin of diamondiferous calcsilicates and gneisses (i.e., "crustal sedimentary" versus "magmatic mantle-derived" protolith) as proposed by Marakushev et al. (1998) and Massonne (2003).

Diamondiferous metamorphic rocks from the Kokchetav Massif (Kazaksthan) are mostly represented by biotite gneisses (85 vol.%) with subordinate dolomite marbles (calcsilicate) and garnet-pyroxene rocks with (or without) carbonates (15 vol.%). The latter rocks have attracted much attention because of their unusual high diamond grade (up to 3,000 carats per metric ton) and variations in garnet and clinopyroxene compositions, even within a single hand specimen (Shatsky et al. 2006a, b; Sobolev et al. 2001, 2007; Schertl et al. 2004). Some rare calcsilicate rock samples are layered and include different lithologies. Dolomite-rich and calcite-rich layers, with minor amounts of garnet and clinopyroxene, may alternate with layers mainly composed of garnet and clinopyroxene (see Schertl et al. 2004, their Fig. 2). Consequently, as a function of the different whole-rock chemistries of the distinct layers, the chemical compositions of minerals also vary widely. These variations are dominantly reflected by Mg# [100 Mg/(Mg + Fe)] of coexisting garnets and clinopyroxenes and in Ca# [100Ca/(Mg + Ca + Fe + Mn)] of garnets (40–80 mol. % grossular). The highest Mg#s (up to 94) of garnets are detected in very rare Mg–Ca garnet relics within dolomite-rich layers. Those garnets generally were found to contain bright-luminescent randomly distributed irregular spots of 50–500 μm in size as well as vein-like structures lacking luminescence (Schertl et al. 2004). The proportions of luminescent areas vary between about 5 and 70% of a grain's cross-section. However, more than 80% of garnet grains from dolomite-rich layers completely lack luminescence. The bright luminescent portions possibly represent an earlier garnet generation, which is characterized by the lowest amounts of iron ever detected (from 1 to 2 wt% FeO) in natural garnets of intermediate pyrope-grossular solid solution (Sobolev et al. 2001, 2007). Such garnets are not stable at pressures below 32 kbar (Boyd 1970), which is also confirmed by diamond presence in xenoliths containing MgCa-garnet from kimberlites (Ponomarenko et al. 1976) as well as by the presence of diamond in the sample of this study. Coesite (Katayama et al. 2002) and magnesite inclusions are found in zircons (Shatsky et al. 1995) from calcsilicates of the Kokchetav Massif, and forsteritic olivine and Ti-clinohumite are found in dolomitic matrix (Schertl et al. 2004; Sobolev et al. 2007).

Oxygen isotope ratios are a valuable tool to constrain the geological environment and to decipher the fluid evolution of UHP metamorphism (Rumble 1998; Valley 1986; Valley et al. 1998, 2005; Valley and Cole 2001; Ohta et al. 2003; Jahn et al. 2003).The aim of the present study is to focus on different generations of garnet uniquely rich in Mg and Ca (which can be clearly distinguished by detailed CL-studies) and to compare them with other garnets of extreme compositional variations observed in different lithologies of the same hand sample and even within a single thin section. We report detailed chemical analysis and in situ oxygen isotope ratios from zoned garnet and coexisting pyroxene in the calcsilicate sample, K-98-8, which exhibits alternating layers with variable amounts of carbonate minerals, garnet, and clinopyroxene.

Geological background

The Kokchetav Massif is located within the Caledonides of the Central Asian fold belt and is represented by dislocated fragments of the pre-Late Riphean Kazakhstan—North Tianshan microcontinent (Zonenshain et al. 1990). The protolith of UHP-metamorphic rocks is a sedimentary rock sequence including carbonate rocks, sandstones, and shales. The structure of the Kokchetav complex is interpreted as a mega-mélange zone that consists of several tectonic units which are separated by tectonic thrusts or faults (Dobretsov et al. 1995).

The UHP-metamorphic rocks from the Kokchetav Massif have attracted a lot of attention during the last two decades since they were the first to be discovered to contain metamorphic microdiamonds included within primary minerals like garnet, clinopyroxene, kyanite, and zircon (Sobolev and Shatsky 1990; Sobolev et al. 1994; Shatsky

et al. 1995). Diamond findings were followed by the discovery of numerous coesite inclusions in zircons (Sobolev et al. 1991, 1994) and garnets (Korsakov et al. 1998; Shatsky et al. 1998). Diamondiferous rocks in the Kumdy–Kol terrane occur as steeply dipping, thin slices (few hundred meters) within granite gneiss (e.g., Sobolev et al. 2003; Dobretsov and Shatsky 2004).

Geothermobarometry based on mineral compositions (Sobolev and Shatsky 1990; Zhang et al. 1997; Shatsky and Sobolev 2003) indicates that peak metamorphic conditions were $P > 40$ kbar and $T \sim 1{,}000$°C (Dobretsov and Shatsky 2004).

Sample description

The sample of this study (K-98-8) was collected from waste dumps of the underground gallery at the Kumdy Kol domain, which is described in detail by Zhang et al. (1997), Sobolev et al. (2001, 2003), Shatsky et al. (1999, 2006a, b), Sitnikova and Shatsky (2009), and Ogasawara (2005). Metamorphic diamond occurs as an inclusion within pyroxene of this sample. The HP-rock to UHP-rock sequence of this locality is of Cambrian metamorphic age (Claoué-Long et al. 1991; Hermann et al. 2006; Ragozin et al. 2009), and is genetically related to Precambrian granite-gneisses and sediments of the Kokchetav microcontinent (Dobretsov et al. 2006). The studied sample shows a clear alternation of dolomite-rich and garnet-clinopyroxene-rich (in Mg-calcite matrix) layers. Dark layers are characterized by dolomite matrix, while light gray layers have Mg-calcite matrix. Both layers including their contact zone are shown in Figs. 1 and 2. Dolomite matrix layers also contain Ti-clinochumite and forsteritic olivine (Schertl et al. 2004; Sobolev et al. 2001), which belong to layer "c" of Fig. 1, but which are out of the field of view of that part of thin section. Several garnets in these layers were studied using cathodoluminescence (CL) microscopy. By CL, internal structures of luminescent minerals can be made visible within seconds (e.g., Schertl et al. 2004, 2005; Harlow and Sorensen 2005). In contrast to earlier described samples of these rocks (Zhang et al. 1997; Shatsky et al. 1995; Ohta et al. 2003; Ogasawara 2005), the hand specimen, K-98-8, contains the two different lithologies and thus represents a "micro outcrop". In this particular sample, no coesite was found; coesite is a very rare even in other calcsilicate hand samples of the same lithology (Katayama et al. 2002).The selected sample is similar to that studied by Schertl et al. (2004) and Sobolev et al. (2007).

Figure 1 shows a photomicrograph of the 2.2 cm studied portion of sample K-98-8, containing the widest range in garnet and pyroxene chemical compositions (Table 1). The contact zone between Mg-calcite matrix and dolomite matrix is about 1 mm wide. We concentrated on three key areas of this sample, which are shown in Fig. 1: (a) Mg-calcite matrix, (b) contact zone, (c) dolomite matrix.

Sample preparation

In order to select garnets and pyroxenes with the maximum range of compositions and to study the contact relations of the different lithologies, a preliminary examination of several thin sections of sample K-98-8 was accomplished. The sample was cut perpendicular to its banding and, as described by Schertl et al. (2004), two contrasting lithologies could be distinguished by cathodoluminescence (CL). The Mg-calcite matrix is characterized by orange luminescence, while the dolomite matrix shows red luminescence. Both layers contain considerable amounts of garnet and pyroxene. The contact zone is shown in thin section in Figs. 1 and 2b. As a first step, a series of Mg-enriched garnets were identified in several thin sections, which display irregular luminescent domains in their cores (generally smaller than 100 μm, Schertl et al. 2004; Sobolev et al. 2001, 2007) were studied by CL microscopy and electron microprobe (EMP). We found one elongated garnet grain (about 0.5 × 2 mm) with a homogeneous luminescent core (Sobolev et al. 2001). Its position in another thin section which is cut parallel to the studied thin section (Fig. 1) is in dolomite matrix, about 1 cm below the boundary with Mg-calcite matrix. Since not all of the garnets show such luminescent domains, we made laser fluorination oxygen isotope (and EMP) studies on mm-scale chips of several garnets and pyroxenes, and compare these results with data derived from other layers of the same hand sample. The garnet grains from different parts of the sample differ in color; thus we were able to distinguish them visually.

Because of the very complex character of the contact zone of the studied sample and the closeness of the different layers to each other, it was not possible to focus on single "layers", using the laser fluorination technique, which requires samples one million times larger in mass (mg vs. ng) than the pits analyzed in situ by ion microprobe. Thus, a part of the sample representing the contact area with both types of carbonate matrices was crushed, and fragments of garnet and pyroxene grains (<0.2 mm) were handpicked. The separates were selected according to color. Whereas pyroxene fragments were partitioned into pale green and more intensely colored fractions, the garnet fragments were subdivided due to their orange (lowest Mg#), reddish, and yellowish (highest Mg#) colors. The pale green pyroxenes and the yellowish garnets belong to the layer with dolomite matrix, the more Fe-rich layer with Mg-calcite matrix hosts the intense-green pyroxenes, reddish orange and orange garnets. Only the yellowish garnets

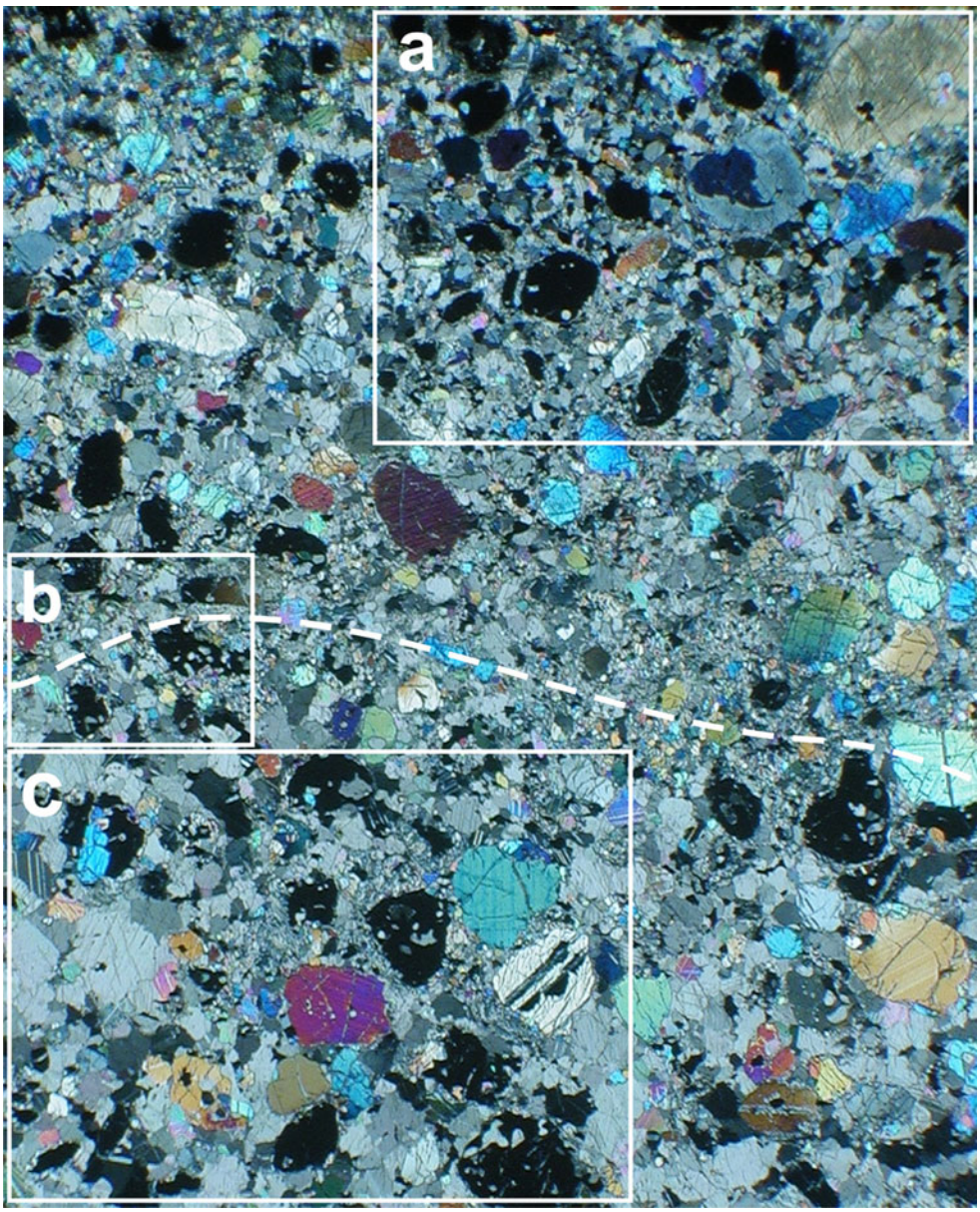

Fig. 1 Photomicrograph of a part of a thin section of a calcsilicate rock (sample K-98-8; crossed polars). The *boxed* areas **a**, **b**, **c** refer to Fig. 2. The field of view is 2.2 cm in vertical long dimension. The *dashed line* separates a layer, which is characterized by Mg-calcite matrix (*top*) from that of dolomite matrix (*bottom*)

that are poor in iron sometimes show luminescent portions. To avoid missing certain garnet and pyroxene compositions from different layers identified in thin section, we handpicked grain fragments from six separates. Gemmy garnet and pyroxene fragments, which did not contain any visible mineral or fluid inclusions were selected using a binocular microscope. In order to be sure that each mineral separate contained only garnets or pyroxenes of the same color, all the grains were cleaned and simultaneously checked at the same field of view under the binocular microscope. During the final preparation of 1–2 mg samples for laser fluorination, grain fragments were additionally cleaned and checked for purity. Fragments from each aliquot analyzed by laser fluorination were studied by EMP (35 grains from each separate).

Analytical techniques

Oxygen isotope ratios ($^{18}O/^{16}O$) were determined with a CAMECA IMS-1280 ion microprobe as well as by laser fluorination at the University of Wisconsin–Madison. Laser fluorination ($\lambda = 10.6$ μm, BrF_5) and gas-source mass–spectrometry of 1–2 mg chips of garnet and clinopyroxene were calibrated using UWG-2 garnet standard as described

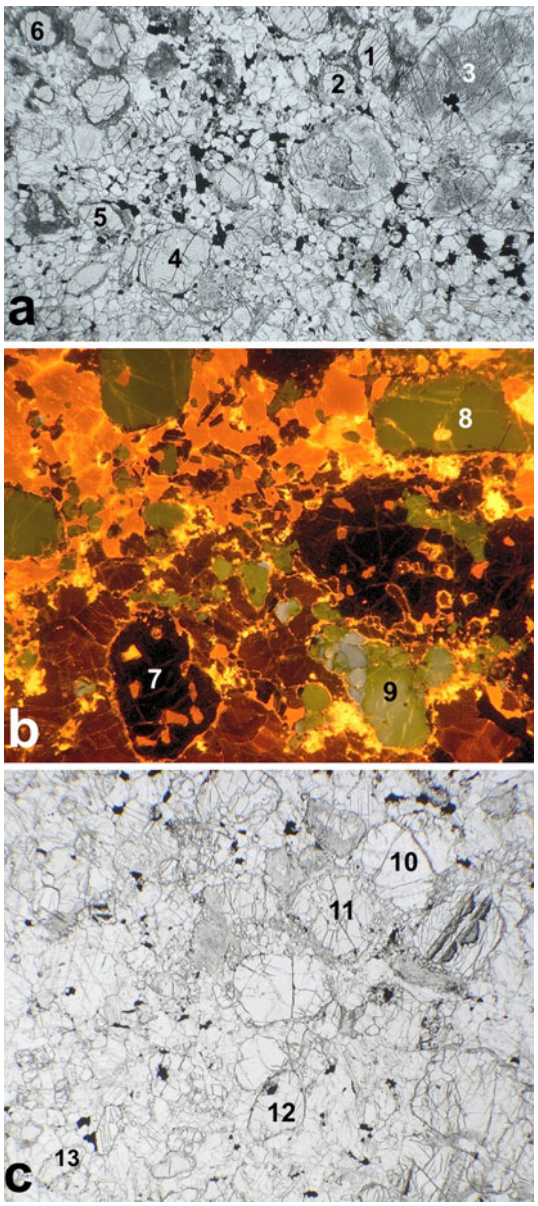

Fig. 2 Photomicrographs from Fig. 1. **a** garnet-pyroxene-rich zone with Mg-calcite matrix; plain polarized light; width of field of view = 1.1 cm. **b** enlarged cathodoluminescence (CL) image of a contact zone between the layer predominantly consisting of dolomite matrix (*bottom; dark red*) with Ti-clinohumite, forsterite, low-iron garnets, and pyroxenes and the one which mainly consists of Mg-calcite matrix (*top, orange*) along with iron-rich garnets and pyroxenes (width of field of view = 4.5 mm), and **c** Fe-poor garnets and pyroxenes embedded in dolomite matrix; plain polarized light; width of field of view = 1.1 cm. Numbers refer to EMP analyses presented in Table 1 (1–13)

by Valley et al. (1995) and are reported in standard per mil format relative to VSMOW (Table 2) along with EMP data for grain fragments from separates.

One elongated, CL-zoned garnet grain (Sobolev et al. 2001) was selected for analysis by ion microprobe. The thin section containing the garnet was ground into a 25-mm diametered disk with the target garnet within 2 mm of the center position. The garnet standard UWG-2 was mounted into the surface of the thin section within 2 mm of the sample garnet and polished to be coplanar with the sample garnet. Ion microprobe analyses were made with a 10 kV $^{133}Cs^{+}$ primary beam and O^{-} secondary beam following procedures described by Kita et al. (2009) and Valley and Kita (2009). The ^{16}O and ^{18}O peaks were analyzed simultaneously using dual Faraday cup detectors. A mass resolution of ~2,500 removed hydride interferences on ^{18}O. The count rate for ^{16}O was typically 3.29×10^9 cps yielding 1.02×10^9 cps/nA. Sample analyses were bracketed by at least 8 analyses of the UWG-2 garnet standard, which yielded spot to spot precision of ±0.2–0.3‰ (2SD).

The cation solid solutions of garnet and other minerals introduce systematic differences in bias of the measured oxygen isotope ratios by ion microprobe, sometimes referred to as the matrix effect (e.g., Vielzeuf et al. 2005; Valley and Kita 2009). In order to correct for this compositional bias, we apply a correction scheme based on the correlation of matrix induced bias and grossular content in Al-rich garnets in a set of secondary garnet standards (Page et al. 2010). We analyzed three secondary garnet standards (Table S1, S2) that compositionally bracket the zoned garnet in Ca–Mg–Fe space. Two standards (near end-member pyrope PypDM and grossular GrsSE) that bracket the sample in Ca and Mg were analyzed during the same session as the zoned garnet (Table S1), a third standard with intermediate Ca, Mg, and Fe was analyzed against UWG-2 in a separate session (Table S2). A calibration curve (Fig. S1) was established using the method of Page et al. (2010). The cation composition of the sample garnet was measured adjacent to each ion microprobe analysis pit by EMP (Table 3), and matrix bias was calculated for each analysis. For these sample compositions, the matrix bias varies between 1.8 and 2.6‰ relative to the UWG-2 standard with larger corrections correlating with increasing Ca concentration. Sample data were corrected in a two-part procedure. First, data were corrected for instrumental bias using the UWG-2 master standard and reported as $\delta^{18}O^{*}$ (Table S1). Then the matrix bias calculated for each analysis relative to UWG-2 was applied yielding a final corrected value reported in ‰ relative to VSMOW. The uncertainty derived from the spot-to-spot reproducibility (±0.2–0.3‰) combined with the estimate of the error in the correction scheme (±0.4‰) yields an estimated combined error of ±0.5‰.

EMP measurements were made using a JEOL 8100 at the Institute of Geology and Mineralogy (Novosibirsk) with an accelerating voltage of 20 kV and current intensity of 30 nA. Simple oxides MgO, Al_2O_3, SiO_2, Fe_2O_3, NiO, rutile (TiO_2), pure diopside, Mn-garnet, albite, and K-feldspar were used as standards. The spot size was about

Table 1 Chemical compositions (EMP analyses) of selected garnets and pyroxenes from different layers of sample K 98-8

Grain#	SiO_2	TiO_2	Al_2O_3	FeO	MnO	MgO	CaO	Na_2O	K_2O	Total	Ca#	Mg#
1	39.9	0.41	21.5	13.5	0.78	6.06	18.3	n.d.	n.d.	100.45	48.3	44.5
2c	39.2	0.34	21.6	15.6	0.85	6.15	16.3	n.d.	n.d.	100.04	43.2	41.2
2r	39.5	0.36	21.4	14.1	0.79	5.64	18.4	n.d.	n.d.	100.19	48.6	41.7
4c	39.3	0.36	21.5	15.2	0.84	6.37	16.5	n.d.	n.d.	100.07	43.6	42.8
4r	39.6	0.31	21.9	12.7	0.79	6.13	18.6	n.d.	n.d.	100.03	49.5	46.3
5c	39.1	0.41	21.5	13.6	0.78	6.25	18.0	n.d.	n.d.	99.66	47.4	45.0
5r	39.1	0.33	21.6	12.2	0.77	5.84	19.7	n.d.	n.d.	99.55	51.9	46.0
6c	39.4	0.38	21.5	14.2	0.79	5.76	18.2	n.d.	n.d.	100.28	48.0	41.9
6r	39.8	0.34	21.6	14.1	0.86	4.79	19.6	n.d.	n.d.	101.05	51.7	37.8
7c	40.9	0.73	21.7	5.23	0.54	9.84	20.2	n.d.	n.d.	99.16	52.6	77.0
7r	41.2	0.62	22.0	5.33	0.61	11.4	18.1	n.d.	n.d.	99.27	47.0	79.2
11	40.8	0.92	21.5	3.77	0.51	9.67	22.0	n.d.	n.d.	99.19	56.7	82.1
12c	41.2	0.15	22.2	2.38	0.76	9.27	23.4	n.d.	n.d.	99.30	60.4	87.4
12r	41.4	0.83	21.9	3.54	0.54	11.7	19.7	n.d.	n.d.	99.54	50.2	85.5
13	41.0	0.75	21.6	3.24	0.56	10.4	21.4	n.d.	n.d.	98.94	55.1	85.1
3c	53.5	0.06	2.65	5.04	0.10	14.2	22.6	1.20	0.15	99.49	48.8	83.7
3r	53.2	0.06	2.95	4.41	0.11	14.5	22.9	1.10	0.13	99.43	49.2	85.4
8c	55.3	0.04	0.86	1.42	0.05	17.5	24.5	0.39	0.06	100.18	49.0	95.7
8r	54.7	0.08	1.94	1.91	0.08	16.7	24.1	0.52	0.02	100.06	49.4	94.0
9c	55.5	0.03	0.74	0.91	0.04	17.8	25.0	0.25	0.05	100.30	49.4	97.2
9r	55.2	0.06	1.04	1.22	0.06	18.4	23.5	0.21	0.19	99.81	46.9	96.4
10	55.5	0.02	0.37	0.66	0.03	18.6	25.1	0.05	0.11	100.41	48.7	98.1
dol (incl)	n.d.	n.d.	n.d.	1.61	0.15	20.6	31.2	n.d.	n.d.	53.56		
dol	n.d.	n.d.	n.d.	1.92	0.17	19.6	30.7	n.d.	n.d.	52.39		
cal	n.d.	n.d.	n.d.	1.43	0.05	4.12	53.0	n.d.	n.d.	58.60		

For the following Tables, Cr_2O_3 and Na_2O in garnets are <0.03 wt%; *c* core of the grain, *r* rim of the grain, *n.d.* not determined

Ca# − [100Ca/(Ca + Mg + Fe + Mn)]; Mg# − [100 Mg/(Mg + Fe)]. Grains 1, 10, 11, and 13 are homogeneous in composition

dol (incl) dolomite inclusion in clinopyroxene, *dol* dolomite from the matrix, *cal* Mg-calcite from the matrix

Table 2 Chemical compositions (EMP analyses) and $\delta^{18}O$-values of fragments of typical garnet and pyroxene grains from separates (1–6) used for laser fluorination

Separate#	SiO_2	TiO_2	Al_2O_3	FeO	MnO	MgO	CaO	Na_2O	K_2O	Total	Ca#	Mg#	Grain color	$\delta^{18}O$ (‰) VSMOW
1 (grt)	41.3	0.80	22.1	2.94	0.72	11.6	19.7	n.d.	n.d.	99.20	50.9	87.6	LY	10.62
2 (grt)	41.1	0.70	21.7	3.56	0.49	9.82	22.2	n.d.	n.d.	99.64	56.9	83.1	Y	10.39
3 (grt)	39.9	0.37	21.6	7.41	0.95	4.40	25.1	n.d.	n.d.	99.75	66.5	51.4	R	8.11
4 (grt)	40.2	0.36	21.5	12.1	0.77	6.16	19.0	n.d.	n.d.	100.07	50.5	47.7	RO	7.00
5 (grt)	39.4	0.39	21.3	15.3	0.76	5.91	16.4	n.d.	n.d.	99.51	44.2	40.7	RO-O	6.33
6 (grt)	39.9	0.35	21.5	13.7	0.84	5.81	17.8	n.d.	n.d.	99.92	47.8	43.0	O	6.29
2a (cpx)	54.9	0.05	0.65	0.92	0.02	17.9	24.5	0.15	0.17	99.23	48.8	97.2	PG	8.07
3a (cpx)	54.4	0.08	2.21	2.67	0.10	15.9	23.4	0.28	0.25	99.25	49.1	91.4	PG-G	8.00
4a (cpx)	54.1	0.05	2.04	3.28	0.10	15.4	23.5	0.69	0.06	99.26	49.4	89.3	G	6.72
5a (cpx)	54.1	0.06	3.57	4.62	0.09	13.6	21.9	1.48	0.28	99.71	49.3	84.0	G-IG	6.32
6a (cpx)	53.9	0.07	2.83	4.26	0.08	14.5	22.4	1.13	0.17	99.37	48.7	85.9	IG	6.11

Grain fragments color in separates

LY is light yellow, *Y* is yellow, *R* is red, *RO* is red–orange, *O* is orange, *PG* is pale green, *G* is green, and *IG* is intensive green, *n.d.* not determined

Table 3 Chemical composition (EMP analyses) adjacent to SIMS pits and corresponding $\delta\ ^{18}O_{VSMOW}$-data of zoned garnet K98-8; c: luminescent part and r: non-luminescent part of the garnet grain

Spot	SiO_2	TiO_2	Al_2O_3	FeO	MnO	MgO	CaO	Total	Ca#	Mg#	$\delta^{18}O$ (‰) VSMOW
9 r	41.5	0.68	22.3	3.12	0.67	12.5	18.6	99.38	47.7	87.7	11.3
10 c	41.7	0.17	22.7	1.19	1.13	10.0	22.6	99.52	59.0	93.7	12.3
12 r	41.4	0.92	22.1	2.94	0.64	11.9	19.7	99.71	50.5	87.8	11.3
13 r	41.1	0.87	21.8	3.04	0.69	11.5	20.0	99.16	51.3	87.1	11.8
14 c	41.7	0.14	22.5	1.31	1.18	10.1	22.7	99.56	58.7	93.2	12.2
15 c	41.5	0.28	22.5	1.34	1.14	10.0	22.5	99.40	58.7	93.0	12.2
16 r	41.6	0.87	22.1	3.11	0.68	11.8	19.5	99.57	50.1	87.1	11.6
21 r	41.5	0.66	22.4	3.20	0.71	13.0	17.9	99.47	45.9	87.9	11.5
22 r	41.8	0.53	22.5	3.29	0.78	13.8	17.1	99.75	43.3	88.2	11.5
23 c	41.6	0.17	22.7	1.23	1.16	10.0	22.7	99.59	58.9	93.5	12.7
24 c	41.6	0.15	22.5	1.22	1.18	9.91	22.6	99.25	59.1	93.5	12.6
25 c	41.4	0.09	22.7	1.24	1.19	9.94	22.8	99.34	59.1	93.5	12.8
26 c	41.4	0.09	22.6	1.21	1.18	9.89	22.8	99.28	59.4	93.6	12.4
27 c	41.7	0.10	22.6	1.21	1.20	9.99	23.1	99.88	59.4	93.6	12.6
28 c	41.5	0.26	22.4	1.36	1.23	9.51	22.9	99.16	60.0	92.6	12.5
29 r	41.6	0.64	22.4	3.23	0.82	13.0	17.8	99.55	45.7	87.7	11.6
30 r	41.4	0.83	22.1	3.03	0.68	12.0	19.3	99.37	49.7	87.5	11.4
31 r	41.8	0.34	22.9	2.98	0.79	12.5	18.6	99.96	47.8	88.2	11.5
32 r	42.1	0.37	23.2	3.37	0.84	13.8	16.6	100.16	42.5	87.9	11.9
33 c	41.6	0.18	22.5	1.44	1.05	10.2	22.5	99.54	58.3	92.7	12.5

2 μm. The relative standard deviation of measurements was less than 1% (Korolyuk et al. 2008).

CL-measurements were performed using a "hot cathode" scanning electron microscope of the type HCL-LM at Ruhr–University Bochum. Operating conditions were 14 keV beam energy and ~9 μA/mm^2 current beam density. For more details, see Neuser (1995) and Schertl et al. (2004, 2005).

Results

Mineral chemistry

The EMP data were measured on both sides of the contact zone dividing two layers, which are dominated by dolomite or Mg-calcite matrices, respectively. The contact zone is indicated by a dashed line in Fig. 1. In Fig. 2b, the contact is also exposed; the dolomite matrix zone is dominated by red luminescence color (bottom), the Mg-calcite matrix zone (top) shows orange CL. The contrasting garnets and pyroxenes that were previously identified by CL microscopy studies are chemically characterized using EMP (see Table 1).

Garnets from Mg-calcite matrix (area "a" in Figs. 1 and 2a) are colored which is visible in thin section. Garnets (#1, 2, 4–6, Fig. 2) are analyzed by EMP (see Table 1). The most pronounced zonation is found for grain 4 with higher FeO content in the core (15.2 wt%) compared to the rim (12.7 wt%). Other grains 2, 5, 6 demonstrate weaker zonation and grain 1 is unzoned which probably is a result of the different levels that grains were cut during thin section preparation. The total range in Mg#′s for these garnet grains is between 37.8 and 46.3 while Ca#′s show only moderate differences from 43.2 to 51.9. The low amounts of TiO_2 (0.31–0.41 wt%) and MnO (0.77–0.85 wt%) are typical for garnets from Mg-calcite matrix. Garnets from dolomite matrix are considerably more magnesian with Mg#′s from 77.0 to 87.4. The analyses of grains 7, 11, 12, and 13 (see Fig. 2) are presented in Table 1. Their Ca#′s are between 47.0 and 60.4 which are higher compared to garnet compositions from Mg-calcite matrix.

Pyroxene #3 from Mg-calcite matrix is enriched in FeO and zoned with Mg# 83.7 in core and 85.4 in the rim (see Table 1). It contains a diamond inclusion. Pyroxenes from dolomite matrix contain considerably lower FeO with Mg#′s between 94.0 and 98.1 (grains 8–10, see Fig. 2 and Table 1). Pyroxenes from both matrixes contain relatively low, but detectable K_2O (0.02–0.19 wt%).

Following the procedure described in "sample preparation", several garnet and pyroxene separates were hand-picked according to color differences and selected grains of each separate were analyzed by EMP (see Table 2). The

grains selected from separates are characterized by the same ranges of Mg# seen in each matrix (43.0–51.4 and 84.0–91.4 for garnet and pyroxene, respectively from Mg-calcite matrix, and 83.1–87.6 and 97.2, respectively from dolomite matrix).

As mentioned above (see sample preparation), special efforts were made to select a garnet grain with homogeneous luminescent zone for SIMS study. After examination of a number of grains, the elongated grain was selected (Fig. 3a). The homogeneity of the grain both was checked by EMP across several analytical profiles and a total of 100 spots (Sobolev et al. 2001, their Fig. 3b). The position of this analyzed garnet grain is close to grains 12 and 13 (Fig. 2c and Table 1) although it occurs in a different thin section.

The wide range of garnet compositions obtained by EMP is nicely expressed by FeO contents varying between 2.38 and 15.6 wt% (Mg# between 87.4 and 41.2). The respective amounts of FeO in different pyroxene grains are between 0.66 and 5.04 wt%. (Mg# between 83.7 and 98.1; Table 1), the single grains only show a very faint zonation. Small amounts of K_2O are detected in different pyroxene grains in thin section (0.02–0.19 wt%) and in separates (0.02–0.28 wt%), which is presented in Tables 1 and 2 (see also grain 3 in Fig. 2, containing diamond inclusions). The compositions of Mg-calcite and dolomite are also presented in Table 1. The yellow luminescent mineral in Fig. 2b is calcite that was introduced along fissures and thus represents a late, secondary carbonate generation. These fissures generally are concentrated directly at the Mg-calcite-matrix/dolomite-matrix boundary. Olivine in dolomite matrix is Mg# 96–97, without CaO and NiO (below detection limit), and with high amounts of MnO (about 0.30 wt%) (Schertl et al. 2004; Sobolev et al. 2001). The mentioned minerals belong to the same layer as in Fig. 2c, but are out of a field of view.

δ^{18}O ion microprobe data

The garnet grain selected for ion microprobe study is elongated and the luminescent inner part does not demonstrate regular growth zonation although it is reminiscent of rim/core-relations described in other studies (Kohn et al. 1993; Clechenko and Valley 2003; Perchuk et al. 2005; Vielzeuf et al. 2005; Page et al. 2010). Figure 3a displays a CL-microphotograph of the luminescent inner and non-luminescent outer parts of the crystal. Figure 3b shows the chemical profile (A–B) of Ca, Mg, Fe, Mn, and Ti per double formula unit (garnet composition is calculated on the basis of 24 oxygens). The ion microprobe spots (numbered white dots) are aligned along the profile A–B. In addition, new EMP analyses have been performed as close as possible to the ion microprobe spots, which was necessary for the correction of the ion microprobe analyses (Table 3). Three additional ion microprobe spots were analyzed outside profile A–B. In total, twenty spot analyses were made, half of which are on the luminescent part of the garnet grain ("c" in Table 3), the other half are on the part lacking luminescence ("r" in Table 3).

Figure 4 shows the values of the δ^{18}O(garnet) that were obtained by ion microprobe along profile A–B. The data, including corrected analyses on samples and standards are presented in Table 3 documenting that the luminescent inner part is characterized by distinctively higher δ^{18}O values between 12.2 and 12.8‰ compared to its non-luminescent rim (11.3–11.9‰).

δ^{18}O laser fluorination data

Figure 4 demonstrates a sharp zonation of oxygen isotope ratios within a single grain and thus a wide range of δ^{18}O-compositions can exist at hand sample scale. In order to put the in situ data in larger context, we sought the

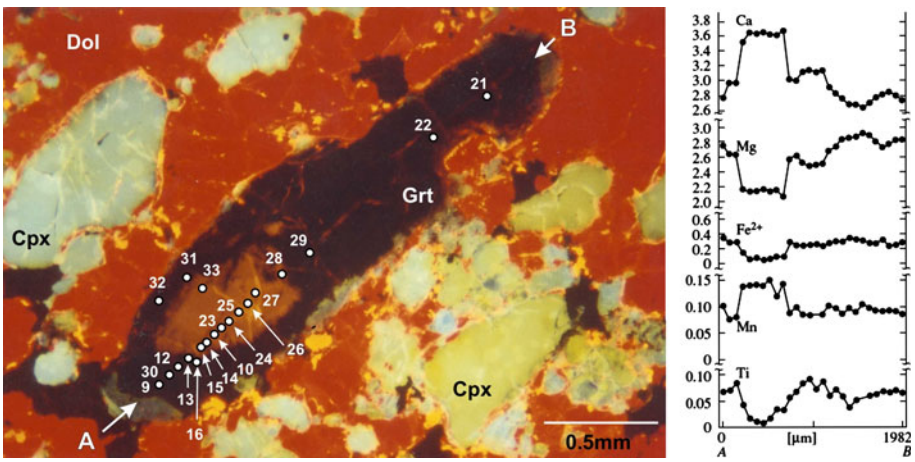

Fig. 3 CL microphotograph (*left*) showing the luminescent inner part and non-luminescent rim of the studied garnet with numbered spots analyzed by ion microprobe (Dol = dolomite, Cpx = clinopyroxene, Grt = garnet). Chemical profile of garnet (*right*); values are in atoms per double formula unit; see Sobolev et al. (2001). Note the absence of any secondary minerals and cracks in this part of thin section

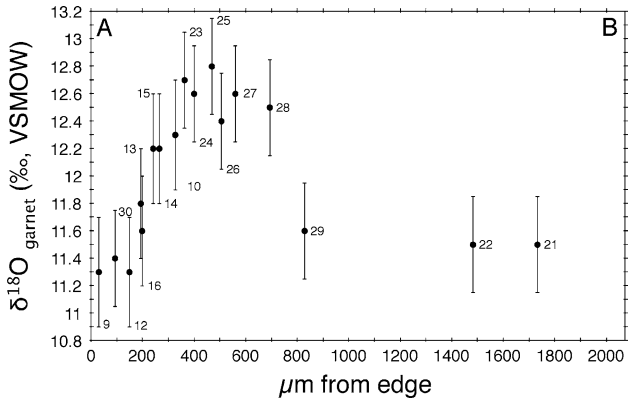

Fig. 4 Profile of $\delta^{18}O$ in garnet shown in Fig. 3 measured in situ at WiscSIMS using a 10 μm spot. *Error bars* (2SD) and distances (x-axis) are indicated

widest possible range of chemical and isotopic compositions by hand-picking six different garnet fractions and five different clinopyroxene fractions (<200 μm) from the crushed rock sample. These mineral separates were then analyzed in bulk (~2 mg/analysis) for $\delta^{18}O$ by laser fluorination (Table 2 and Fig. 5) and selected grains from each separate were studied by EMP (see also Table 2).

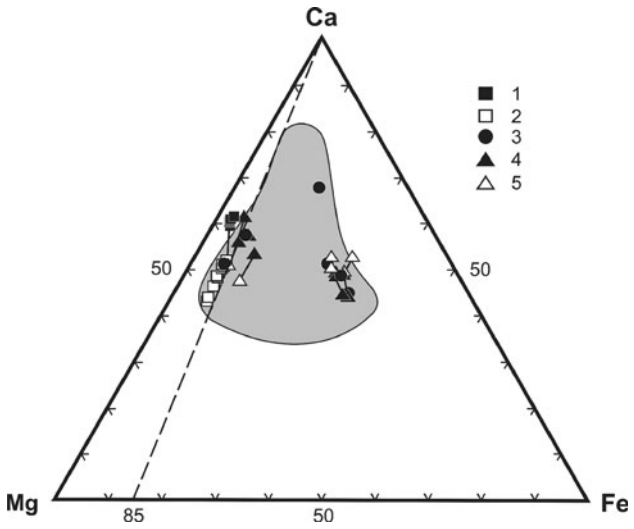

Fig. 5 Composition of Mg–Ca(Fe) garnets from sample K-98-8. Symbols for garnet grain analyzed in situ atWiscSIMS are: (1) for luminescent inner part; (2) for non luminescent rim; (3) garnet compositions from mineral separates used for laser fluorination analyses. Symbol 4 (*filled triangle*) refers to core analyses of garnet grains from thin section (Fig. 2) numbered 1, 2, 4–7, 11, 12, 13 in Fig. 2. Symbol 5 refers to the respective rims of the same garnets (cores and rims of the same grains are connected with *tie lines*). Shaded area represents the compositional range of garnets from the series of calcsilicate and garnet-pyroxene rocks from Kokchetav Massif (Sobolev et al. 2007). Dashed line corresponds to garnet compositions with Mg# 85, which indicates the limits in Mg# for the overwhelming majority of garnets from UHP mantle and crustal rocks (Sobolev et al. 2001)

The oxygen isotope analyses of six garnet fractions chosen for laser fluorination are in the range of $\delta^{18}O = 10.6–6.3‰$. These values are lower than the unusually zoned grain selected for in situ analysis. This difference is real; it correlates with the different chemical compositions. Most likely, the differences in $\delta^{18}O$ reflect preservation of primary, or nearly primary, compositions in the garnet core and the layered character of the sample. The chemistries of garnets and clinopyroxenes also vary widely. Comparing the results of the EMP analyses of garnets from different layers of the studied sample, two separate clusters of Mg# (Grt) can be observed (Fig. 5). While the low Mg-garnets (Mg# 37.8–46.3) belong to the Mg-calcite layer, the high Mg-garnets (Mg# 77.0–87.4) belong to the dolomite layer. The compositions of the luminescent inner part of the garnet grain analyzed by SIMS and also those of the non-luminescent rim (symbols 1 and 2 of Figs. 5, 6) are characterized by highest Mg-numbers (see Table 1 for analyses). However, several EMP analyses of the zoned garnet used for SIMS (analyses 7 c, r; 11, 12, c, r, see Table 1) are very close in Mg# to those of garnet fragments from the separates analyzed by laser fluorination, and thus occupy a similar position in Fig. 5 (e.g. symbol 3). Similarly, as seen from Fig. 5, the marked points of garnet grains 2, 4, 6 (see Fig. 2; Table 1) overlap with those of samples 4, 5, 6 used for laser fluorination study (see Table 2).

Table 2 shows the $\delta^{18}O$ values measured by laser fluorination for garnet and pyroxene separates that were hand-picked by color. Although the different lithologies are only a few mm thick (see Fig. 1), we tried to achieve pure separates of six different portions of the studied sample (Table 2). In separates 1 and 2 (Table 2), garnet fragments with high $\delta^{18}O$ values (ca 10.5‰) were found, whereas similar high $\delta^{18}O$ pyroxene fragments were not found. Values of $\delta^{18}O$ for fragments in garnet separate no. 3 (8.1‰; Table 2) are within the range of those of pyroxenes available from separates 2 and 3. Note that separates numbered 2 and 2a, 3 and 3a, etc., are pairs (see Table 2) that came from sub-samples with the same number. In separates 4, 5, and 6, both garnet and pyroxene show nearly identical $\delta^{18}O$ values. These garnets and coexisting pyroxenes are approximately in isotopic equilibrium. It should be noted, however, that these analyses average compositions at the mm-scale and that it is not possible to avoid small amounts of mixing of lithologies.

Figure 6a shows $\delta^{18}O$ values versus Mg#s of garnets. This presentation of data was selected because Mg# often correlates with $\delta^{18}O$ values for garnets from crustal versus mantle genesis (e.g., Schulze et al. 2003; Spetsius et al. 2008; Vielzeuf et al. 2005). Mg# and Ca# for many garnets (xenoliths, diamond inclusions and UHP-metamorphic rocks) completely overlap in Mg–Fe–Ca diagrams. Figure 6b

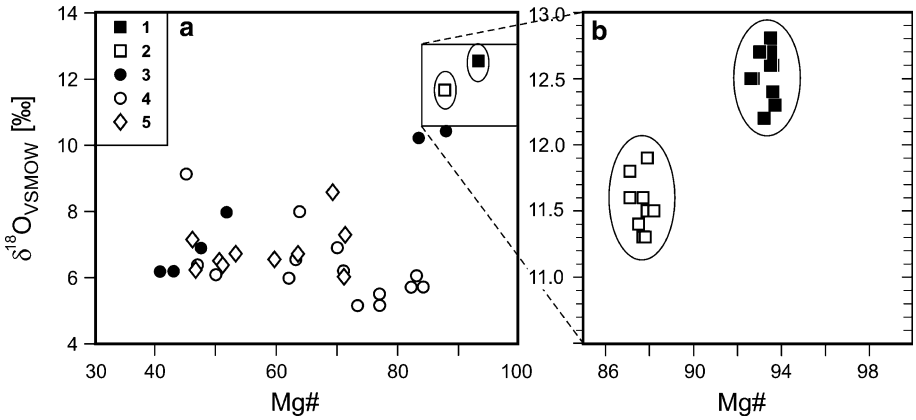

Fig. 6 Relations between Mg# and $\delta^{18}O$ of some UHP garnets of mantle and crustal origin. **a** Ion microprobe data (1, 2) and laser fluorination data (3) of garnets from sample K-98-8 (this study). Laser fluorination data of garnet xenocrysts (4) from Venezuela kimberlites (Schulze et al. 2003) and laser fluorination data (5) of garnets from diamondiferous eclogites of the Nyurbinskaya pipe, Yakutia (Spetsius et al. 2008). **b** = enlarged portion of (**a**); error (2SD) is 0.4‰

shows an enlarged portion of Fig. 6a with garnets of the highest Mg# and $\delta^{18}O$ values measured by ion microprobe along the profile of Figs. 3 and 4.

Discussion

Sample K-98-8 represents the full range of lithology and compositions in a single thin section (Fig. 1) of these most unusual rocks known from this locality. It contains a calcsilicate rock with dolomite matrix, in contact with a garnet-pyroxene rock with a Mg-calcite matrix. Both rock types contain associated garnets and pyroxenes of wide compositional ranges and are characterized by a high diamond grade with diamonds occurring as inclusions in garnets, pyroxenes, (see Fig. 2 grain no. 3) and zircons. It should be noted that in other descriptions of these two lithologies in UHPM rocks, they are separate blocks (e.g., Shatsky et al. 1995; Zhang et al. 1997; Ogasawara 2005). The oxygen isotope data demonstrate a large 6‰ range in $\delta^{18}O$ for garnets from 12.8 down to 6.3‰, preserved within a single hand sample of layered calcsilicate rock marked by dolomite and Mg-calcite matrices with variable amounts of garnets and pyroxenes.

Pyroxene-spinel symplectites with scarce sapphirine and corundum developed around pyrope-grossular garnet analyzed by EMP in sample K-98-8 (Sobolev et al. 2001) and similar rocks (Schertl et al. 2004) indicate granulite facies conditions (experimentally confirmed by Massonne, 1995) during an initial stage of exhumation. Hydrous retrograde minerals (e.g., zoisite, phlogopite, low-Si phengite), both in symplectites and in the rock matrix, were not observed in sample K-98-8. Examining a wide series of diamond-bearing carbonate rocks from Kokchetav Massif by studying O, C and Sr isotope geochemistry, Ohta et al. (2003) showed alteration due to percolation of fluids through fractures and along grain boundaries at the time of retrograde metamorphism during exhumation. They noted the wide distribution of hydrous minerals replacing high-grade silicate assemblages and particularly drew attention on low $\delta^{18}O$ and $\delta^{13}C$ values for these rocks (9 and −9‰, respectively) as well as on high $^{87}Sr/^{86}Sr = 0.8050$. Their study concluded that coexisting dolomite and Mg-calcite during UHP metamorphism rarely preserve equilibrium compositions, and only in samples isolated from infiltrating fluids by distance from fractures. However, Ohta et al. (2003) randomly selected dolomite marbles containing silicate minerals and only the typical geochemical features of these rocks were discussed. Sample K-98-8 differs from dolomite marbles examined by Ohta et al. (2003) and represents an unusually well-preserved precursor that was relatively protected from infiltrating retrograde fluids.

The role of fluids

The lack of hydrous minerals in the studied sample (except of some minor Ti-clinohumite) and the presence of "dry" symplectitic rims around garnets with luminescent cores as well as around similar garnets of other samples (Schertl et al. 2004; Sobolev et al. 2001) suggests that fluids were limited or absent at the peak (UHP to granulite facies) temperatures of these rocks. Fluids causing alteration must thus have been late stage. Earlier IR spectroscopic study of garnets from a calcsilicate rock of the Kokchetav Massif suggested the presence of defect OH groups corresponding to those in synthetic OH bearing pyropes (Langer et al. 1993). The variability of IR spectra of garnets with low H_2O contents suggests that the hydrogarnet substitution is not the only means of incorporating OH groups (Beran and Libowitzky 2006). All analyzed garnets and pyroxenes in

this study were checked for purity and homogeneity to avoid any mineral or fluid inclusions. Hwang et al. (2005) and Dobrzhinetskaya et al. (2005) used TEM and AEM techniques to identify a highly potassic COH fluid with dissolved phosphate, chloride, and sulfate/sulfide forming nanometer-size inclusions in microdiamonds of calcsilicate and garnet-pyroxene rocks from Kokchetav Massif.

De Corte et al. (1998) demonstrated the presence of water and carbonate inclusions in microdiamonds from garnet-pyroxene rocks of the Kokchetav Massif; their observations appear to be similar to those derived from cloudy Yakutian kimberlitic diamonds (e.g., Klein–Ben David et al. 2009). The discovery of nanometer-size to micrometer-size inclusions of dolomite sometimes associated with phlogopite in metamorphic (Dobrzhinetskaya et al. 2006) and kimberlitic diamonds (Logvinova et al. 2008; Sobolev et al. 2009), and the direct experimental evidence obtained for diamond crystallization from a silicate-carbonate melt/fluid (Pal'yanov et al. 1997, 2001, 2002) argue for the presence of a carbonate melt in equilibrium with a K-rich fluid for diamond formation, both in crustal metamorphic rocks and in mantle environment (Shatsky et al. 2005; Pal'yanov et al. 2007). Experiments by Luth (1997) demonstrate that the formation of phlogopite associated with garnet and clinopyroxene is confined to PT-conditions within the diamond stability field. Thus, fluid (melt) inclusions in Kokchetav microdiamonds may have been trapped during (or close to) peak metamorphic conditions at mantle depths similar to those that occur in kimberlitic diamonds.

Constraints from oxygen diffusion

The zoned garnet in this study contains an apparently symmetric gradient of 1.5‰/200 μm in $\delta^{18}O$ as constrained by ion microprobe analysis (Figs. 4, 7). If the zonation in this garnet formed prior to or during the peak of metamorphism, then any initial gradient would be relaxed by diffusion of oxygen isotopes both within the garnet and between the garnet and its dolomite matrix (see, Page et al. 2010). In order to evaluate this constraint, we constructed a simple, one-dimensional, isothermal diffusion model assuming that the isotopic zonation was formed as a step between a core with $\delta^{18}O = 12.8‰$ (the highest measured value located centrally in the core region) and a rim of 11.3‰ (the average value of analyses in the non-luminescent rim region). It is then possible to calculate the set of curves that would result from diffusion between the core and rim of the garnet using equation 3.45 of Crank (1975). Figure 7 shows a detail of the oxygen isotope traverse across the narrow rim and into the core of the garnet from Fig. 4. Superimposed on the data are the predicted diffusion profiles calculated for a temperature of 1,000°C

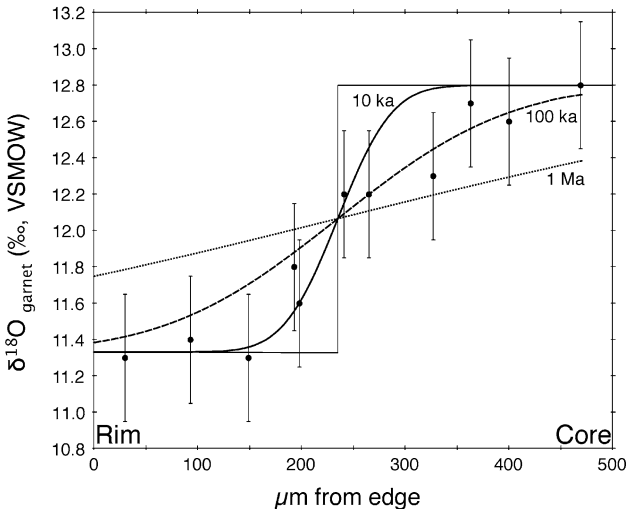

Fig. 7 Enlargement of in situ ion microprobe analyses of $\delta^{18}O$ (garnet) made at WiscSIMS from Fig. 4. The curves were calculated assuming diffusive relaxation of a 1.5‰ step in $\delta^{18}O$ using a 1-D model at 1,000°C for the times shown. A gradient of this magnitude would not be preserved for 1 million years and most likely formed due to late fluid infiltration at the end, or after, the peak of metamorphism (see text)

(Dobretsov and Shatsky 2004), using the experimentally determined diffusion constant of Coghlan (1990). If the zoning in $\delta^{18}O$ in this garnet had formed before or during the peak of metamorphism, the profile as measured could not have survived for 1 My, even in the absence of exchange during cooling. In fact, these results indicate that heating was for a time period 1 to 2 orders of magnitude shorter in duration and that uplift was very rapid. Given the depths to which these rocks were buried, these constraints suggest that the zonation in this garnet formed in response to late fluids after the peak of metamorphism, consistent with textural observations made using CL. Although this diffusion model is simplified, in this case, the assumptions made are all conservative: diffusion from the second and third dimension, a non-step starting condition, a prolonged period of cooling after the peak of metamorphism, and diffusion into the garnet from the dolomite matrix containing 1.6 wt% FeO would all serve to increase the amount of diffusive relaxation observed for a given period of time.

Conclusions

The high $\delta^{18}O$ values (up to 12.8‰) in the luminescent inner portion of the zoned garnet in sample K-98-8 are significantly higher than would be in equilibrium with mantle-derived magmas and indicate formation in, or exchange with, a crustal reservoir. Trace element data for diamondiferous calcsilicate rocks from the Kumdy Kol

deposit and the results of carbon and nitrogen isotope studies and nitrogen abundance of Kokchetav microdiamonds further support a metasedimentary origin.

The different $\delta^{18}O$ values of garnets and pyroxenes in the different lithologies may reflect initial heterogeneity of the sedimentary precursors. It is of particular importance, however, that the variations in $\delta^{18}O$ located within a single zoned garnet crystal (Figs. 3, 4) require fluid-mediated oxygen isotope exchange. Although some of the luminescent garnet patches show an irregular distribution, the luminescent core of Fig. 3 may represent a relic of the prograde stage and could not be interpreted to have formed by late-stage influx of fluids. The low $\delta^{18}O$ alteration of the garnet in this study may have formed close to the peak of metamorphism but, if so, metamorphism and uplift must have been rapid as the diffusion rate of oxygen in garnet at 1,000°C is too fast to preserve the measured $\delta^{18}O$-gradient of 1.5‰/200 μm for long period of time.

Acknowledgments We thank W. Faryad, R. Abart, V.V. Reverdatto and Y.-F. Zheng for helpful comments on an earlier version of the manuscript and two anonymous reviewers for their detailed suggestions related to the present version. We gained a lot from the experience of Jochen Hoefs, the editor—thank you for your valuable suggestions and final review. Fruitful discussions with Doug Rumble helped improve clarity of the results. The WiscSIMS laboratory at the University of Wisconsin is partly supported by NSF-EAR (0319230, 0744079) and DOE (93ER14389). We are grateful to R. Lehmann (RUB) for drafting work.

References

Beran A, Libowitzky E (2006) Water in natural mantle minerals II: olivine, garnet and accessory minerals. In: H Keppler, JR Smyth, eds. Rev Mineral Geochim 62:169–191

Boyd FR (1970) Garnet peridotites and the system $CaSiO_3$–$MgSiO_3$–Al_2O_3. Mineralo Soci Am Special Publi 3:63–75

Chopin C, Sobolev NV (1995) Principal mineralogic indicators of UHP in crustal rocks. In: Coleman RG, Wang X (eds) Ultra-high pressure metamorphism. Cambridge Univ Press, Cambridge, pp 96–131

Claoué-Long JC, Sobolev NV, Shatsky VS, Sobolev AV (1991) Zircon response to diamond-pressure metamorphism in the Kokchetav Massif, USSR. Geology 19:710–713

Clechenko CC, Valley JW (2003) Oscillatory zoning in garnet from Willsboro wollastonite skarn, Adirondack Mts, NY: a record of shallow hydrothermal processes preserved in a granulite facies terrane. J Metamorph Geol 21:771–784

Coghlan RAN (1990) Studies in diffusional transport: grain boundary transport of oxygen in feldspars diffusion of oxygen, strontium and the REEs in garnet and thermal histories of granitic intrusions in south-central Maine using oxygen isotopes. Ph.D. Diss, Brown University

Crank J (1975) The mathematics of diffusion. Oxford University Press, New York, p 414

De Corte K, Cartigny P, Shatsky VS, Sobolev NV, Javoy M (1998) Evidence of fluid inclusions in metamorphic microdiamonds from the Kokchetav Massif, northern Kazakhstan. Geochim Cosmochim Acta 62:3765–3773

Dobretsov NL, Shatsky VS (2004) Exhumation of high-pressure rocks of the Kokchetav Massif: facts and models. Lithos 78:307–318

Dobretsov NL, Sobolev NV, Shatsky VS, Coleman RG, Ernst WG (1995) Geotectonic evolution of diamondiferous paragenesis, Kokchetav Complex, Northern Kazakhstan: the geologic enigma of ultrahigh-pressure crustal rocks within a Paleozoic foldbelt. The Island Arc 4:267–279

Dobretsov NL, Buslov MM, Zhimulev FI, Travin AV, Zayachkovsky AA (2006) Vendian-early Ordovician geodynamic evolution and model for exhumation of ultrahigh and high-pressure rocks from the Kokchetav subduction-collision zone (northern Kazakhstan). Russ Geol Geophys 47:424–440

Dobrzhinetskaya LF, Wirth R, Green HW (2005) Direct observation and analysis of a trapped COH fluid growth medium in metamorphic diamond. Terra Nova 17:472–477

Dobrzhinetskaya LF, Wirth R, Green HW (2006) Nanometric inclusions of carbonates in Kokchetav diamonds from Kazakhstan: a new constraint for the depth of metamorphic diamond crystallization. Earth Planet Sci Lett 243:85–93

Harlow GE, Sorensen SS (2005) Jade (nephrite and jadeitite) and serpentinite: metasomatic connections. Intern Geol Rev 47: 113–146

Hermann J, Rubatto D, Korsakov AV, Shatsky VS (2006) The age of metamorphism of diamondiferous rocks determined with SHRIMP dating of zircon. Rus Geol Geophys 47:513–520

Hwang SL, Shen P, Chu HT, Yui TF, Liou JG, Sobolev NV, Shatsky VS (2005) Crust-derived potassic fluid in metamorphic microdiamond. Earth Planet Sci Lett 231:295–306

Jahn B-M, Rumble D, Liou JG (2003) Geochemistry and isotope tracer study of UHP metamorphic rocks. In: Carswell DA, Compagnoni R (eds) EMU notes in mineralogy, vol 5, pp 365–414

Katayama I, Ohta M, Ogasawara Y (2002) Mineral inclusions in zircons from diamond-bearing marble in the Kokchetav Massif, northern Kazakhstan. Eur J Mineral 14:1103–1108

Kita NT, Ushikubo T, Fu B, Valley JW (2009) High precision SIMS oxygen isotope analyses and the effect of sample topography. Chem Geol 264:43–57

Klein-Ben David O, Logvinova AM, Schrauder M, Spetius ZV, Weiss Y, Hauri EH, Kaminsky FV, Sobolev NV, Navon O (2009) High-Mg carbonatitic microinclusions in some Yakutian diamonds—a new type of diamond-forming fluid. Lithos 112S2: 648–659

Kohn MJ, Valley JW, Elsenheimer D, Spicuzza MJ (1993) O isotope zoning in garnet and staurolite: evidence for closed-system mineral growth during regional metamorphism. Am Mineral 78: 988–1001

Korolyuk VN, Lavrentév YG, Usova LV, Nigmatulina EN (2008) JXA-8100 microanalyzer: accuracy of analysis of rock-forming minerals. Russ Geol Geophys 49:165–168

Korsakov AV, Shatsky VS, Sobolev NV (1998) The first finding of coesite in eclogites of the Kokchetav Massif. DoklAkad Nauk 360:77–81 (in Russian)

Langer K, Robarick E, Sobolev NV, Shatsky VS, Wang W (1993) Single-crystal spectra of garnets from diamondiferous high-pressure metamorphic rocks from Kazakhstan: indications for OH^-, H_2O and FeTi charge transfer. Eur J Mineral 5:1091–1100

Logvinova AM, Wirth R, Fedorova EN, Sobolev NV (2008) Nanometer-sized mineral and fluid inclusions in cloudy Siberian diamonds: new insights on diamond formation. Eur J Mineral 20:317–331

Luth RW (1997) Experimental study of the system phlogopite-diopside from 3.5 to 17 GPa. Am Mineral 82:1198–1209

Marakushev AA, Paneyakh NA, Zotov IA (1998) The problem of mantle petrology. Geol Geofiz (Russ Geol Geophys) 39: 1750–1755 (1740–1745)

Massonne H-J (1995) Experimental and petrogenetic study of UHPM. In: Coleman RG, Wang X (eds) Ultrahigh pressure metamorphism. Cambridge University Press, UK, pp 33–95

Massonne HJ (2003) A composition of the evolution of diamondiferous quartz-rich rocks from the Saxonian Erzgebirge and the Kokchetav Massif: are so-called diamondiferous gneisses magmatic rocks? Earth Planet SciLett 216:347–364

Mattey DP, Lowry D, Macpherson CG, Chazot G (1994) Oxygen isotope composition of mantle minerals by laser fluorination: homogeneity in peridotites, heterogeneity in eclogites. Min Mag 58A:573–574

Neuser RD (1995) A new high-intensity cathodoluminescence microscope and its application to weakly luminescing minerals. Bochumer geol geotechArbeiten 44:116–118

Ogasawara Y (2005) Microdiamonds in ultrahigh-pressure metamorphic rocks. Elements 1:91–96

Ohta M, Mock T, Ogasawara Y, Rumble D (2003) Oxygen, carbon, and strontium isotope geochemistry of diamond-bearing carbonate rocks from Kumdy-Kol, Kokchetav Massif, Kazakhstan. Lithos 70:77–90

Page FZ, Kita NT, Valley JW (2010) Ion microprobe analysis in garnets of complex chemistry. Chem Geol 270:9–19

Pal'yanov YN, Khokhryakov AV, Borzdov YM, Sokol AG, Gusev VA, Rylov GM, Sobolev NV (1997) Growth conditions and real structure of synthetic diamond crystals. Geol Geofiz (Russ Geol Geophys) 38:882–918 (920–945)

Pal'yanov YN, Shatsky VS, Sokol AG, Tomilenko AA, Sobolev NV (2001) Crystallization of metamorphic diamond: an experimental modeling. Dokl Earth Sci 381:935–938

Pal'yanov YN, Sokol AG, Borzdov YUM, Khokhryakov AF, Sobolev NV (2002) Diamond formation through carbonate-silicate interaction. Am Mineral 87:1009–1013

Pal'yanov YUN, Shatsky VS, Sobolev NV, Sokol AG (2007) The role of mantle ultrapotassic fluids in diamond formation. Proc Natl Acad of Sci of the USA 104:9122–9127

Perchuk AL, Burchard M, Maresch WV, Schertl H-P (2005) Fluid-mediated modification of garnet interiors under ultrahigh-pressure metamorphism. Terra Nova 17:545–553

Ponomarenko AI, Sobolev NV, Pokhilenko NP, Lavrent'ev YG, Sobolev VS (1976) Diamond-bearing grospydite and kyanite eclogites from the Udachnaya pipe, Yakutia. DoklAkad Nauk SSSR 226:158–161 (in Russian)

Ragozin AL, Liou JG, Shatsky VS, Sobolev NV (2009) The timing of the retrograde partial melting in the Kumdy-Kol region (Kokchetav Massif, Northern Kazakhstan). Lithos 109:274–284

Rumble D (1998) Stable isotope geochemistry of ultrahigh-pressure rocks. In: Hacker BR, Liou JG (eds) When continents collide: geodynamics and geochemistry of ultrahigh-pressure rocks. Kluwer Academic Publishers, Dordrecht, pp 241–259

Schertl H-P, Neuser RD, Sobolev NV, Shatsky VS (2004) UHP-metamorphic rocks from Dora Maira/Western Alps and Kokchetav/Kazakhstan: new insights using cathodoluminescence petrography. Eur J Mineral 16:49–57

Schertl H-P, Medenbach O, Neuser RD (2005) UHP-metamorphic rocks from Dora Maira, Western Alps: Cathodoluminescence of silica and twinning of coesite. Russ Geol Geophys 46:1327–1332

Schulze DJ, Valley JR, Bell DR, Spicuzza MJ (2001) Oxygen isotope variations in Cr-poor megacrysts from kimberlite. Geochim Cosmoch Acta 65:4375–4384

Schulze DJ, Valley JW, Spicuzza MJ, de Channer DMR (2003) The oxygen isotope composition of eclogitic and peridotitic garnet xenocrysts from the La Ceniza kimberlite, Guaniamo, Venezuela. Intern Geol Rev 45:968–975

Shatsky VS, Sobolev NV (2003) The Kokchetav Massif of Kazakhstan. In: Carswell DA, Compagnoni R (eds) "Ultrahigh pressure metamorphism". EMU notes in Mineralogy, vol 5, pp 75–103

Shatsky VS, Sobolev NV, Vavilov MA (1995) Diamond-bearing metamorphic rocks of Kokchetav Massif (Northern Kazakhstan). In: Coleman RG, Wang X (eds) Ultrahigh pressure metamorphism. Cambridge University Press, UK, pp 427–455

Shatsky VS, Theunissen K, Dobretsov NL, Sobolev NV (1998) New indications of ultrahigh-pressure metamorphism in the mica schists of the Kulet site of the Kokchetav Massif (north Kazakhstan). Geol Geofiz (Russ Geol Geophys) 39:1039–1044 (1041–1046)

Shatsky VS, Jagoutz E, Sobolev NV, Kozmenko OA, Parkhomenko VS, Troesch M (1999) Geochemistry and age of ultrahigh pressure metamorphic rocks from the Kokchetav Massif (Northern Kazakhstan). Contrib Mineral Petrol 137:185–205

Shatsky VS, Pal'yanov YN, Sokol AG, Tomilenko AA, Sobolev NV (2005) Diamond formation in UHP dolomite marbles and garnet-pyroxene rocks of the Kokchetav Massif, Northern Kazakhstan: natural and experimental evidence. Intern Geol Rev 47:999–1010

Shatsky VS, Ragozin AL, Sobolev NV (2006a) Some aspects of metamorphic evolution of ultrahigh pressure calc-silicate rocks of the Kokchetav Massif. Russ Geol Geophys 47:105–119

Shatsky VS, Sitnikova ES, Kozmenko OA, Palessky SV, Nikolayeva IV, Zayachkovskiy AA (2006b) Behavior of incompatible elements during ultrahigh-pressure metamorphism (by the example of rocks of the Kokchetav Massif). Russ Geol Geophys 47:485–498

Sitnikova ES, Shatsky VS (2009) New FTIR spectroscopy data on the composition of the medium of diamond crystallization in metamorphic rocks of the Kokchetav Massif. Russ Geol Geophys 50: 842–849

Sobolev NV, Shatsky VS (1990) Diamond inclusions in garnets from metamorphic rocks: a new environment for diamond formation. Nature 343:742–745

Sobolev VS, Sobolev NV (1980) New evidence of the sinking to great depths of the eclogitized rocks of Earth crust. Dokl Akad Nauk SSSR 250:683–685

Sobolev NV, Yefimova ES, Koptil VI, Lavrent′ev YG, Sobolev VS (1976) Inclusions of coesite, garnet and omphacite in diamonds of Yakutia-first find of coesite paragenesis. Dokl Akad Nauk SSSR 230:1442–1444 (in Russian)

Sobolev NV, Galimov EM, Ivanovskaya IN, Yefimova ES (1979) Isotopic composition of carbon of diamonds containing crystalline inclusions. Dokl Akad Nauk SSSR 249:1217–1220

Sobolev NV, Shatsky VS, Vavilov MA, Goryainov SV (1991) Coesite inclusion in zircon from diamondiferous gneiss from Kokchetav Massif–first find of coesite in metamorphic rocks in the USSR territory. Dokl Akad Nauk 321:184–188 (in Russian)

Sobolev NV, Shatsky VS, Vavilov MA, Goryainov SV (1994) Zircon from ultra high pressure metamorphic rocks of folded regions as an unique container of inclusions of diamond, coesite and coexisting minerals. Dokl Akad Nauk 334:488–492 (in Russian)

Sobolev NV, Schertl H-P, Burchard M, Shatsky VS (2001) An unusual pyrope-grossular garnet and its paragenesis from diamondiferous carbonate silicate rocks of the Kokchetav Massif, Kazakhstan. Dokl Earth Sci 380:791–794

Sobolev NV, Shatsky VS, Liou JG, Zhang RY, Hwang SL, Shen P, Chu HT, Yui TF, Zayachkovsky AA, Kasymov MA (2003) US-Russian Civilian Research and Development Fund Project: an origin of microdiamonds in metamorphic rocks of the Kokchetav Massif, Northern Kazakhstan. Episodes 26:290–294

Sobolev NV, Schertl H-P, Neuser RD, Shatsky VS (2007) Relict unusually low iron pyrope-grossular garnets in UHPM calc-silicate rocks of the Kokchetav Massif, Kazakhstan. Intern Geol Rev 9:717–731

Sobolev NV, Logvinova AM, Efimova ES (2009) Syngenetic phlogopite inclusions in kimberlite-hosted diamonds: implications for role of volatiles in diamond formation. Russ Geol Geophys 50:1234–1248

Spetsius ZV, Taylor LA, Valley JW, De Angelis MT, Spicuzza M, Ivanov AS, Banzeruk VI (2008) Diamondiferous xenoliths from crustal subduction: garnet oxygen isotopes from the Nyurbinskaya pipe, Yakutia. Eur J Mineral 20:375–385

Valley JW (1986) Stable Isotope geochemistry of metamorphic rocks. In: Valley JW, Taylor HP, O'Neil JR (eds) Stable Isotopes in high temperature geological processes, vol 16. Mineralogical Society of America, Washington, DC, pp 445–489

Valley JW (2003) Oxygen isotopes in zircon. In: Hanchar JM, Hoskin PWO (eds) Zircon. Reviews in mineralogy and geochemistry, vol 53, pp 343–385

Valley JW, Cole DR (2001) Stable isotope geochemistry. Rev Mineral Geochem 43:662

Valley JW, Kita NT (2009) In situ oxygen isotope geochemistry by ion microprobe. In: Fayek M (ed) MAC short course: secondary ion mass spectrometry in the earth sciences, vol 41, pp 19–63

Valley JW, Kitchen N, Kohn MJ, Niendorf CR, Spicuzza MJ (1995) UWG-2, a garnet standard for oxygen isotope ratios: strategies for high precision and accuracy with laser heating. Geochim Cosmochim Acta 59:5223–5231

Valley JW, Kinny PD, Schulze DJ, Spicuzza MJ (1998) Zircon Megacrysts from Kimberlite: oxygen isotope heterogeneity among mantle melts. Contrib Mineral Petrol 133:1–11

Valley JW, Lackey JS, Cavosie AJ, Clechenko CC, Spicuzza MJ, Basei MAS, Bindeman IN, Ferreira VP, Sial AN, King EM, Peck WH, Sinha AK, Wei CS (2005) 4.4 billion years of crustal maturation: oxygen isotopes in magmatic zircon. Contrib Mineral Petrol 150:561–580

Vielzeuf D, Champenois M, Valley JW, Brunet F, Devidal JL (2005) SIMS analyses of oxygen isotopes: matrix effects in Fe-Mg-Ca garnets. Chem Geol 223(4):208–226

Zhang RY, Liou JG, Ernst WG, Coleman RG, Sobolev NV, Shatsky VS (1997) Metamorphic evolution of diamond-bearing rocks from the Kokchetav Massif, northern Kazakhstan. J Metamorph Geol 15:479–496

Zonenshain LP, Kuzmin MI, Natapov LM (1990) Geology of the USSR: a plate tectonic synthesis. Geodyn Monogr Ser, Am Geophys Union, Washington, DC 242